Multimed Tools Appl (2018) 77:22857–22873
https://doi.org/10.1007/s11042-018-5976-7

Ridge–based curvilinear structure detection for identifying road in remote sensing image and backbone in neuron dendrite image

Fanqiang Kong[1] · **Vishnu Varthanan Govindaraj**[2] · **Yu-Dong Zhang**[3]

Received: 1 December 2017 / Revised: 29 March 2018 / Accepted: 4 April 2018 /
Published online: 27 April 2018

Abstract The curvilinear structure detection is widely applied in many real tasks, such as the fiber classification, river finding, blood vessel detection, and so on. In this paper, we proposed to use the ridge-based curvilinear structure detection (RCSD) for the road extraction from the remote sensing images. First, we employed the morphology trivial opening operation to filter out almost all the small clusters of noise and the small paths. Then RCSD was used to find the road from the remote sensing images. The experiments showed that our proposed method is efficient and give better results than the current existing road-detection methods. Considering the similar structure between backbone in the neuron dendrite images and the road in remote sensing images, we extended the application of RCSD to the backbone detection in neuron dendrite images. The results on backbone detection also proved the efficiency of RCSD.

Keywords Ridge-based curvilinear structure detection · Road detection · Remote sensing · Backbone detection · Neuron dendrite

✉ Fanqiang Kong
kongfq@nuaa.edu.cn

✉ Vishnu Varthanan Govindaraj
g.vishnuvarthanan@klu.ac.in

✉ Yu-Dong Zhang
yudongzhang@ieee.org

[1] College of Astronautics, Nanjing University of Aeronautics and Astronautics, Nanjing, China

[2] Department of Instrumentation and control Engineering, Kalasalingam University, Srivilliputtur, Virudhunagar, Tamil Nadu, India

[3] Department of Informatics, University of Leicester, Leicester LE1 7RH, UK

1 Introduction

Curvilinear structure detection (CSD) becomes an essential procedure in many practical tasks. Such as the fiber classification, river finding, blood vessel detection, free-way traffic patterns and so on. Silva, Martins [34] extracted the filament and tree like structures which forms the blood vessels in medical images based on the curvilinear structure detection. Shih and Kowalski [33] used curvilinear structures to detect the stars and galaxies formed filament-like structure in cosmological data. There are some other applications such as remote sensing and seismology. Martínez and Ludeña [27] and Stanford and Raftery [35] tried to detect curvilinear structures in noisy images. Einbeck and Dwyer [13] employed curvilinear structure identification to analyze the freeway traffic patterns. Dong and Mcavoy [11] applied curvilinear structure for processing monitoring. Su, Srivastava [36] used curvilinear structure identification for shape analysis in point clouds of 2D and 3D.

One of the most famous methods of CSD was proposed by Trevor Hastie [37]. The authors defined the "*principal curves*" as the middle axis, which passes the sample points in a specified way. However, some researchers thought the "principal curve" did not consider self-intersection and multiple curves, hence, scholars added strict assumptions to solve above problem. Typically, locally defined variants of principle curve was proposed by Ozertem and Erdogmus [29]. Furthermore, Pulkkinen [31] proposed a nonparametric estimation of marginal density method, and named it ridge-based curvilinear structure detection (abbreviated as RCSD).

In this paper, we make a tentative study of applying the newly-proposed RCSD to two applications: road detection and backbone detection, because of following reasons. (i) The roads from the remote sensing images may have multiple sub-roads; (ii) The backbone from dendrite image also have multiple dendrites; (iii) nonparametric is easy to implement and does not need to set hyperparameters. Therefore, we apply RCSD to these two fields.

The rest of the paper was organized as follows: Section 2 introduced the related work of road detection and the dendrite extraction. Section 3 described the method of RCSD. Section 4 described the road detection result by RCSD method from the remote sensing images. Section 5 described the backbone detection result by RCSD method from the neuron dendrite images. Section 6 provided the conclusion.

2 Related work

2.1 Road detection

With the development of the autonomous vehicles, the road detection has attracted more and more attentions from researchers. Recently, researchers have proposed various road detection methods.

For example: Barsi and Heipke [4] used a feed-forward neural network for road junction detection. They extracted raster and vector information as the features. The developed systems can automatically and accurately classify the samples as road junction or not. Kong, Audibert [20] presented a scheme to detect road from a single image. They firstly estimated the vanishing point and extracted main parts of the road. Then, the exact boundaries were obtained based on texture orientations and edge detection technique. Li, Zhang [22] put forward a system to detect road edges in remote sensing images of high resolution. Instead of revised parallel-beam radon transform and ridgelet transform, they used traditional edge detection

operators. The proposed method can effectively detect straight road edges. A shadow-invariant feature space was proposed and a classification model was online trained to improve the adaptability of the system to the lighting and vehicles in the current images. Compared to the hue-saturation-intensity based algorithms, their method obviously has better performance. Guo, Mita [16] developed an advanced driver-assistance system. The road detection problem was regarded as a maximum posteriori problem based on Markov random field. They employed an optimization algorithm to label the samples as road or background. Álvarez, López [1] firstly estimated the priors to get the initial information about the road. Then, they extracted features from the image, including low-level cues and contextual cues. Finally, a generative model was trained to detect road borders. Byun, Seo [5] presented a road detection algorithm without the assumption that the surface of road is flat. They extracted spatial and visual context based on Markov random field, and converted the detection problem into a classification problem. Zhou, Kong [43] presented a road detection algorithm for unmanned aerial vehicle. Initially, the road region was obtained by graph cut based detection algorithm. Then, the road areas were tracked using a homograph based road tracking method. Li, Ding [23] proposed a road detection method for the autonomous navigation system. The proposed method first segment the rough road region based on the dark channel, then, three effective soft voting rules were used to distinguish the road from the segmented region.

However, those proposed method highly relied on the resolution of the image and can be easily affected by the noise. The survey is shown in Table 1. Therefore, in this paper, we proposed to use the ridge based curvilinear structure detection method to extract the road from the remote sensing images.

2.2 Backbone detection

For the neuron dendrite images, the backbone detection method can be summarized as two types: Semiautomatic method, which is based on software and needs to be revised manually in

Table 1 Review of state-of-the-art road detection methods

Author	Description of Method	Review
Barsi and Heipke [4]	used a feed-forward neural network for road junction detection	The operator was improved by additional features considering parallelism information of roads in junctions.
Kong, Audibert [20]	detect road from a single image	Exact boundaries were obtained based on texture orientations and edge detection technique
Li, Zhang [22]	used traditional edge detection operators, and proposed a shadow-invariant feature space	their method has better performance than traditional methods.
Guo, Mita [16]	developed an advanced driver-assistance system	The road detection problem was transformed to a maximum posteriori problem based on Markov random field
Álvarez, López [1]	a generative model was trained to detect road borders	they extracted low-level cues and contextual cues.
Byun, Seo [5]	extracted spatial and visual context based on Markov random field	without the assumption that the surface of road is flat
Zhou, Kong [43]	Road detection for unmanned aerial vehicle	the road region was obtained by graph cut based detection algorithm
Li, Ding [23]	road detection method for the autonomous navigation system	three effective soft voting rules were used to distinguish the road from the segmented region

the final step, and another type is automatic method. For example, the SynD was proposed by for dendrite and synapse characteristics analysis in immune-fluorescence images. NeuronJ was proposed to trace the growing of the dendrite. NeuronIQ [28] was proposed for the co-focal multi-photon laser scanning.

Other automatic methods include follows: Koh, Lindquist [19] proposed to extract the dendrite backbone as the medical axis. Xu, Cheng [40] proposed a global threshold based method to segment the image, and then the centerline of the dendrites are extracted by the medical axis transform. Cheng, Zhou [10] used an adaptive threshold to the local contrast for the discrimination of the foreground which includes the spine and dendrite. Fan, Zhou [14] and Zhang, Zhou [42] used the second order derivative method to locate the medical axis of the dendrite backbone. Fan, Zhou [14] used an adaptive local binary fitting energy level set model to find the boundary of the dendrite. Their method is suitable for Alzheimer's disease patients. Zhang, Zhou [42] build a classifier using Linear Discriminate Analysis (LDA) to classify the attached spines into valid and invalid types. Chen [6] proposed a three-step cascaded algorithm-RTSVM, which is composed of ridge detection and Twin Support Vector Machine (TSVM) classifiers for spine classification. Li and Cattani [21] proposed a method based on Wavelet Packet Entropy and Fuzzy Support Vector Machine. Fan, Zhou [15] gave a method based on curvilinear structure detector (CSD).

Those proposed methods for the dendrite location have good performance on the existed dendrite images. However, those methods either have strict assumptions of single dendrite or highly depend on the resolution of the images, as shown in Table 2. In order to overcome those limitations, we proposed a new method in this paper for the dendrite location, and for building the relationship between dendrite location and the road extraction from the remote sensing images.

Table 2 Review of state-of-the-art backbone detection methods

Author	Description of Method	Review
Koh, Lindquist [19]	extract the dendrite backbone as the medical axis	an automatic and geometric approach for detecting and quantifying the 3D structure of dendritic spines, from scanning of laser scanning microscopy
Xu, Cheng [40]	a global-threshold based method	the centerline of the dendrites are extracted by the medical axis transform
Cheng, Zhou [10]	help neurobiologists obtain quantitative morphological information	an adaptive threshold to the local contrast for the discrimination of the foreground which includes the spine and dendrite
Fan, Zhou [14]	an automated approach for detecting spines and tracking spine evolution over time	used the second order derivative method to locate the medical axis, used an adaptive local binary fitting energy level set model to find the boundary
Zhang, Zhou [42]	automated detection of dendritic spines in neuron images	build a classifier using Linear Discriminate Analysis to classify the attached spines into valid and invalid types
Chen [6]	Morphological analysis of dendrites and spines	a three-step cascaded algorithm-RTSVM, combining ridge detection and Twin Support Vector Machine classifiers for spine classification
Li and Cattani [21]	Classify mushroom, stubby, and thin types	an approach based on the combination of wavelet contour analysis for the backbone detection, wavelet packet entropy, and fuzzy support vector machine for the spine classification.

3 Methodology of RCSD

In this paper, we proposed to use ridge-based curvilinear structure detection (RCSD) to estimate the possible generating function to describe the curvilinear structure from the original images. The advantages of RCSD are two folds: (i) It takes self-intersection and multiple curves into account. (ii) It is a nonparametric estimation of marginal density method. Mathematically, RCSD is described below.

The preprocessed gray image was normalized to the binary image. Then, we assumed that the observed samples either belong to background clutter or the main line, which is considered as curvilinear structures [31]. The sample points are expressed as random variables as formulation (1):

$$R = \begin{cases} 0 \\ 1 \end{cases}, \text{the observed sample belongs to} \begin{cases} \text{the background clutter} \\ \text{the curvilinear structure} \end{cases} \tag{1}$$

where R represents for the sample points of the observed variable X in certain compact domain $\Omega \in R_d$. The probabilities of the observed samples are shown as (2):

$$\begin{aligned} P(R=1) &= a \\ P(R=0) &= 1-a \end{aligned} \tag{2}$$

a is set within the range of [0 1], and the sample points of the background clutter is thought as uniformly distributed in the domain of $\Omega \in R_d$.

The generating function of the main line is described as:

$$\{f_i\}_{i=1}^{n} \tag{3}$$

in which, n stands for the number of the main lines. The generating function is defined as a continuous mapping from the compact and connected domain $D_i \subset R$. The function f_i is set as a unit length parameterization for all $i = 1, 2, \ldots, n$. When $R = 1$, the output of the function f will depend on three parameters i, Ψ, and b. i is used to figure out which line the sample points belong to. The variable Ψ represents for the coordinate along the specified lines. Considering that the additive noise of the generating functions, b is defined as the noise. We set

$$P(i) = w_i, w_i > 0 \text{ and } \sum_{i=1}^{n} w_i = 1 \tag{4}$$

and $b \sim N(0,\partial^2)$, which means that the noise has zero mean and variance of ∂^2. According to the above defined parameters, the output of X is expressed as:

$$X|(T = 1, i, \Psi = \varphi) = f(\varphi) + b \tag{5}$$

The density of x is:

$$p_x(x|T = 1, i, \Psi = \varphi) = \frac{1}{\left(\sqrt{2\pi}\varphi\right)^d} \exp\left(-\frac{\|x - f_i(\varphi)\|^2}{2\varphi^2}\right) \tag{6}$$

All the lines in an image are expressed as the set

$$F = \{f_i(\varphi), i = 1, 2, \ldots, n, \text{and } \varphi \in D_i\} \tag{7}$$

However, for the practical applications, there is no prior knowledge about the data generating process available. Therefore, in this paper, we used the non-parametric estimation method, which was directly from the samples obtained from the observed variable X. It means that the density for X has very weak or no relationship with parameters i, Ψ, and b.

We employed the joint density, then via marginalizing. The obtained density will only depends on the variable X instead of i, Ψ, and b. Based on the relationship of the joint and conditional density, we can get (8).

$$\begin{aligned} P_{x,T,i,}(x,R,i,\Psi) &= P_x(x|R=1,i,\Psi=\varphi)P_{T,I,\Psi}(R=1,i,\varphi) \\ &= P_x(x|R=1,i,\Psi=\varphi)P_\Psi(\varphi|i)P_{T,I}(R=1,i) \\ &= P_x(x|R=1,i,\Psi=\varphi)P_\Psi(\varphi|i)P(i)P(R=1) \end{aligned} \tag{8}$$

for $R=0$, we can get the density as

$$p_{x,T,I,}(x,0,i,\Psi) = p_x(x|T=0)\times p(T=0) \tag{9}$$

Here, $p_{x,R,I}(x, 0, i, \varphi)$ means the joint density. Then the joint density is accumulated over on the domains of the variables R, φ and i.

As marginalizing the joint density can make the function in-depend on the prior parameters i, Ψ, and b, the marginal density is expressed as

$$p_x(x) = \frac{\rho}{\left(\sqrt{2\pi}\varphi\right)^d}\sum_{i=1}^{n} w_i \int_{P_i} \exp\left(-\frac{\|x-f_i(\varphi)\|^2}{2\varphi^2}\right) D_\Psi(\varphi|i)\mathrm{d}\varphi + \frac{1-a}{V(\Omega)} \tag{10}$$

Here, $V(\Omega)$ is the volume of domain Ω.

The ridge curve is composed of ridge points, which are defined as local maximums on the cross section of the density with respect to the hyper-plane spanned by a subset of the hessian matrix. In order to implement the estimation of the marginal density, we used the kernel density estimation as it can work without prior knowledge about the data generating process. In this paper, we chose the Gaussian kernel density, which estimates $\hat{P}$ based on a set of samples

$$Y = \{y_i\}_{i=1}^{N} \subset R^2 \tag{11}$$

of the probability density P

$$\hat{P} = \frac{1}{N}\sum_{i=1}^{N} K_H(x-y_i) \tag{12}$$

in which K_H stands for the Gaussian kernel density with a positive and symmetric kernel bandwidth in the domain $R^2 \rightarrow [0,\infty]$, and $H \in R^{2x2}$.

The ridges are separated by assuming that they only locate in the high probability density area. We set the threshold ς to separate the low probability density area and high probability density area. According to the above formulation, we need to first find modes of $\hat{P}$, then take the modes as the initial points to build the ridge point set to get the ridge curve based on these modes. According to the truth that the ridge points are those mode that lie on a ridge curve. The pseudo code of RCSD is shown in Table 3, and the flowchart is presented in Fig. 1.

As there are still some branch lines connecting to the main line, spurs are excluded based on the principle that there only exists one main connected ridge curve component passing through the intersection point. Therefore, the other branch lines passing through such an intersection point are split into different parts.

Table 3 Pseudocodes of RCSD

Step 1	Construct a collection of discrete approximations of component curves
Step 2	Find a set of modes of $\hat{P}$, which are used as starting points
Step 3	Based on these modes as the initial point, extract a part of a ridge curve component.
Step 4	Based on Eq. (13), which works as the predictor-corrector adapted to the initial value, the system can be described as: $\frac{\mathrm{d}}{\mathrm{d}\varphi}\{P(x(\varphi)) \times \nabla^2 P(x(\varphi)) \times \frac{\mathrm{d}}{\mathrm{d}\varphi}\} = 0, x(0) = x_0$ (13)
Step 5	A given point is projected onto the m-dimensional ridge set of the density estimate $\hat{P}$. In this paper, the m is set to be 2.
Step 6	According to the threshold ς, the low-density area separates the ridge curve sets.

4 RCSD for road detection

The problem existing for the road detection based on the remote sensing images incudes that the sensor type can affect the image characteristic in some way. Meanwhile, weather, light,

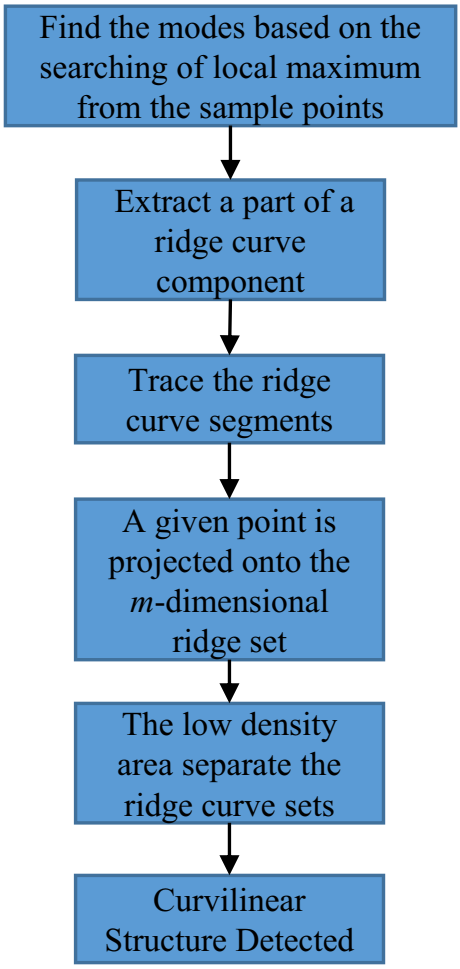

Fig. 1 Flow chart of the ridge-based curvilinear structure detection

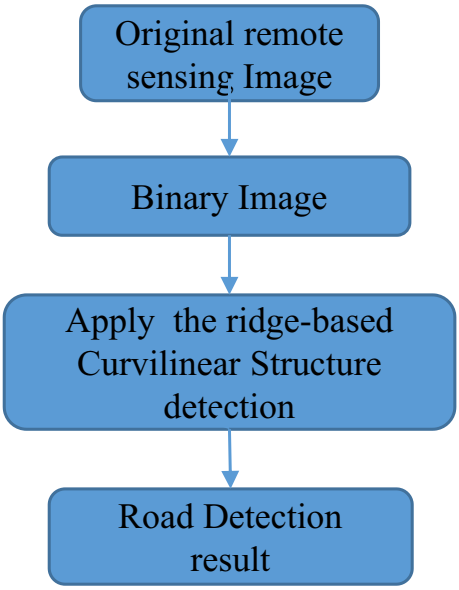

Fig. 2 Pipeline of RCSD for road detection

dust in the air and spectral can affect the remote image sensing. In order to reduce the impact from the sensors and improve the detection precision, we proposed a robust method based on the RCSD to extract the road. However, considering the noise during the imaging, we first employed the morphology trivial opening operation, which filters out nearly all the small clusters of noise and the small paths. The detail information of the morphology trivial opening operation is described as follows.

4.1 Preprocessing

The morphological opening operation can be expressed as:

$$E \circ D = (E \ominus D) \oplus D \tag{14}$$

in which, E and D are sets in Z^2. Equation (14) is termed of the dilation of the erosion of a set E by a structure element D. Erosion is expressed as (15)

$$E \ominus D = \left\{ x | (D)_x \subseteq E \right\} \tag{15}$$

in which, x stands for sets element. Erosion also can be expressed in the form as the duality of the erosion-dilation relationship as formulation (16).

$$E \ominus D = \left(E^c \oplus \hat{D} \right)^c \tag{16}$$

in which, E^c represents for the complement of set E.

Dilation is defined as

$$E \oplus D = \left\{ x | \left(\hat{D} \right)_x \cap E \neq \varnothing \right\} \tag{17}$$

(a) Original image (b) Binarization (c) Detection result

Fig. 3 Road detection from high-resolution remote sensing images

where $\hat{D}$ is obtained by inverting set D. Ø represents for empty set. Formulation (17) means the dilation of set E by D. Dilation can also be expressed as B is inverted first, then translated by x, which can make set E to intersect with $\hat{D}$ by at least of one element.

4.2 Experiments and results

Automatic road detection is important for the town planning, GPS navigation, traffic management, map updating, GPS navigation and autonomous vehicles. Currently, the road detection mainly relies on the manual extraction and semiautomatic method. However, it is a time-consuming operation and hard to repeat. Therefore, considering its importance, a lot of researchers contributed to find solutions of this problem. For the low-resolution images, the road is described more like lines. For the high resolutions images, the road looks like elongated regions with parallel boundaries. In this paper, we mainly focused on the remote sensing images, with the pipeline of our experiment shown in Fig. 2.

Figure 3 shows an example of high-resolution images. There are buildings and roads. First, we transferred the gray image into binary images, and then based on the ridge detection, the road is extracted from the remote sensing images as shown in Fig. 3(c). Figure 4 shows an example with lower resolutions, we can find that in Fig. 4(c) some pixels belonging to the road are missed as the pixel intensity is similar with the other components. As the resolution in Fig. 4 is much lower than Fig. 3, it is hard to distinguish the road pixel from the other buildings. Meanwhile, the road pixel is quite similar with the background information,

(a) Original image (b) Binarization (c) Detection result

Fig. 4 Road detection from low-resolution remote sensing images

Table 4 The confusion matrix of road detection using our RCSD method

Detected class	Road	Non-road
Actual class	(19465)	(168473)
Road	18,207	356
Non-road	792	168,117

therefore, the road pixels are taken as the background information when transferring to the binary images.

In order to test the precision of the proposed algorithm, we detected road from different resolution images, which include road in mountains and plain areas around cities as well as rural as shown in Figs. 3 and 4. The data includes 50 images with 19,465 road pixels.

Table 4 shows that there are 19,465 road pixels and 168,473 non-road pixels in total. There are 18,207 road pixels and 168,817 non-road pixels are correctly detected. We defined four parameters TP, TN, FP, FN as shown in Table 5 and employed the accuracy, specificity, sensitivity and precision to measure the performance of the proposed algorithm.

The accuracy (*Acc*), specificity (*Spec*), sensitivity (*Sen*) and precision (*Prc*) are expressed as Eq. (18)–(21).

$$Acc = \frac{\mathrm{TP} + \mathrm{TN}}{\mathrm{TP} + \mathrm{FP} + \mathrm{FN} + \mathrm{TN}} \tag{18}$$

$$Sen = \frac{\mathrm{TP}}{\mathrm{TP} + \mathrm{FN}} \tag{19}$$

$$Spec = \frac{\mathrm{TN}}{\mathrm{TN} + \mathrm{FP}} \tag{20}$$

$$Prc = \frac{\mathrm{TP}}{\mathrm{TP} + \mathrm{FP}} \tag{21}$$

The measurement of the road detection is shown in Table 6. The accuracy, specificity, sensitivity and precision achieved 99.10%, 99.53%, 98.08% and 93.50% respectively, which means that we correctly detected 18,207 pixels from 19,465 road pixels.

In order to test the performance of the proposed method, we compared our RCSD method with state of the art methods: Long, Shelhamer [25] proposed to apply the fully connected network for the pixel wise application. Badrinarayanan, Kendall [3] used the

Table 5 the physical meaning of the four basic parameters

Parameters	Full name	Physical meaning
TP	True Positive	Road pixels are detected as road pixels
TN	True Negative	Non-road pixels are detected as non-road pixels
FP	False Positive	Non-road pixels are detected as road pixels
FN	False Negative	Road pixels are detected as non-road pixels

Table 6 The measurements of the road detection

Measurements	Values
No. of total road pixels	19,465
Rate of correct detection pixels	18,207
Acc	99.10%
Spec	99.53%
Sen	98.08%
Prc	93.50%

Table 7 Comparison result of the state of the art methods by precision

	FCN [25]	Segnet [3]	GANS [32]	RCSD (Our)
Prc	0.8432	0.8673	0.9237	0.9350

deep convolutional encoder-decoder method named as Segnet for the scene segmentation. Shi, Liu [32] proposed to use the Generative Adversarial Networks (GANs) for the road pixel detection.

The results are listed in Table 7 and Fig. 5. Obviously our RCSD method achieves the greatest value. The reason is: FCN [25] produced the segmentation map highly relied on the resolution. Segnet [3] and GAN [32] made more mistakes on the boundary on the road detection, since they are more suitable for classification other than segmentation.

5 RCSD for backbone detection

Extracting linear features has been widely applied for the roads, railroad, and river of satellite or aerial imagery. The structure of the backbone in neuron dendrite image is similar to the road from the remote sensing images. Therefore, we choose the neuron dendrite as the representation of the biomedical images. We proposed to extend the application to detect backbone from

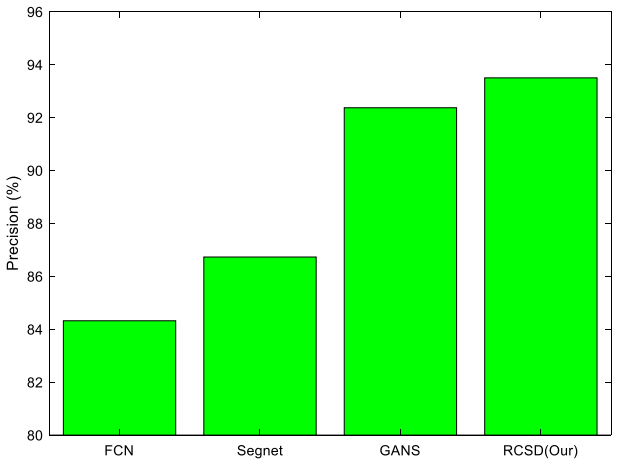

Fig. 5 Comparison of methods of road detection

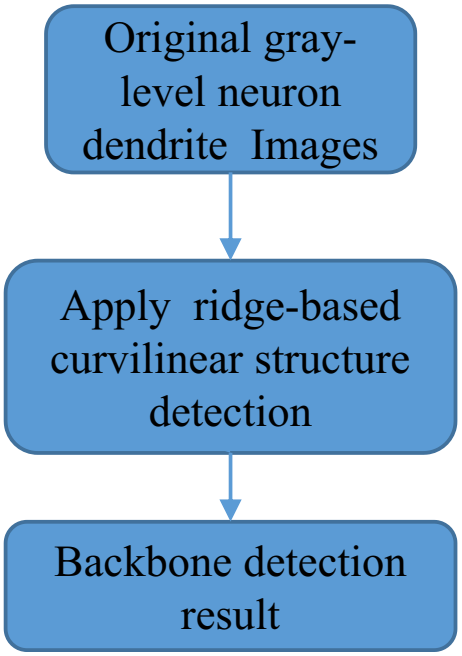

Fig. 6 Pipeline of RCSD for backbone detection

the neuron dendrite images. However, in order to explore the application of the RCSD, we will try more types of images in our future research, such as the blood vessel and so on.

5.1 Background

The dendrites are defined as the neuron branch [9]. It works as to transmit the electrochemical stimulation from other neural cells to the cell body or soma of their parent body. Dendrites received electronic stimulation from upstream neurons via the synapses. Dendrite works as a key role in integrating the inputs from the synapses and in make decision on the extent to which action potentials are produced by the neuron. The morphology of dendrites including the branch density and grouping patterns has a strong relationship with the function of the neuron. Furthermore, the impaired nervous system function is highly related with the malformation of dendrites. Therefore, the detection of the dendrite and quantity analysis is important

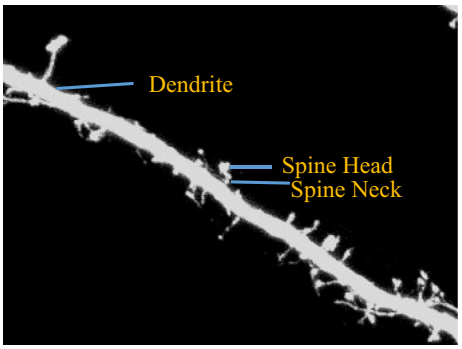

Fig. 7 Sample of a neuron dendrite image (Backbone detection is our aim)

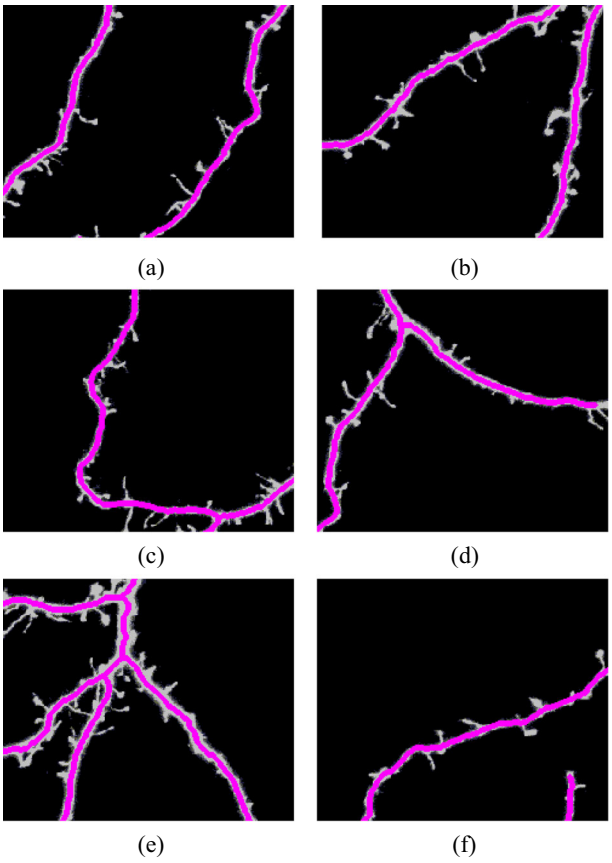

Fig. 8 Backbone detection results. (a) contains two nearly parallel dendrite branches. (b) has two non-parallel dendrite branches. (c) has a single main branch with a small subbranch. (d) presents a diverge takes place along a main branch. (e) shows a multi-branch dendrite. (f) gives two isolated dendrite branches

for the statistics analysis for the biology analysis and build the function map of the function of the neuron and the morphology of the dendrite. Figure 6 provides the pipeline of our experiment applying RCSD for backbone detection.

The research shows that the dendrite growth is tightly correlated with the learning and memory formation. Figure 7 shows an example of one neuron dendrite image. It is composed of dendrite (the main axis from top left to bottom right) and the spine attached to the dendrite. In this paper, our research will focus on the backbone detection. The backbone is the skeleton of the dendrite.

Table 8 Different methods for the backbone detection from 15 sample (Unit: μm)

Method	Length Detected	Gap
Ground Truth	1502.74	0.00%
CSA [9]	1451.63	3.42%
SOD [42]	1435.81	4.45%
CSD [15]	1402.40	6.68%
RCSD (Proposed)	1476.32	1.76%

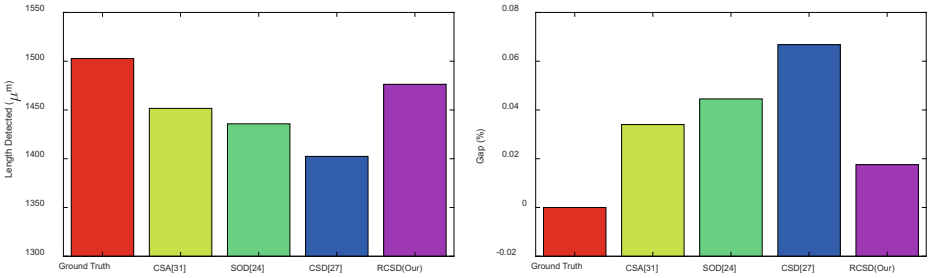

(a) Length detected (b) Gap

Fig. 9 Comparison of backbone detection in terms of relative difference

5.2 Experiments and results

Figure 8 shows different cases of the backbone location, including different numbers of the dendrite and whether has self-intersection. The result shows that the method used for the road detection from the remote sensing images can also be applied for the neuron dendrite detection.

In order to test the proposed algorithm, we proposed to compare our method used in this paper with the second order derivative (SOD) [42], conditional symmetric analysis (CSA) [9], and curvilinear structure detector (CSD) [15]. The comparison results are listed in Table 8. By the length of the detected dendrite, 1476.32 μm was obtained by RCSD, 1451.63 was obtained by CSA [9], 1435.81 was obtained by the second order derivative [42], and 1402.40 was obtained by CSD [15]. The relative difference (i.e., gap) was obtained for four algorithms: 3.42% by CSA [9], 4.45% by Second order derivative [42], 6.68 by CSD [15], and only 1.76% by proposed RCSD. It is obvious that the result of proposed RCSD is closer to the ground truth result. Figure 9 shows the bar-plot of the comparison in terms of length detected and gap.

Although this RCSD was developed for curvilinear structure detection, it may be used in other academic and industrial fields, such as traffic sign detection [30], pathological brain detection [2, 26], path planning [12, 38], hearing loss detection [7], tea category identification [17, 24, 39], breast cancer detection [8], multiple sclerosis detection [41], cerebral microbleeding identification [18], etc.

6 Conclusion

In this study, we proposed a method based on the ridge-based curvilinear structure detection (RCSD) to detect the road pixels from the remote sensing images, and to detect backbone areas from neuron dendrite images. We randomly selected 50 images, which includes 19,465 road pixels and 18,207 road pixels were corrected detected. The precision of RCSD achieved 93.5%. It proved that the proposed algorithm is effective for the road detection from the remote sensing images. Meanwhile, in order to extend the application of the RCSD, we tested the neuron dendrite images from the laser scanning microscopy. The experiments indicated the gap result of RCSD is only 1.76%, which is superior to state-of-the-art approaches.

Acknowledgements This work was supported by National Natural Science Foundation of China (61401200 & 61602250), Open Fund of Guangxi Key Laboratory of Manufacturing System & Advanced Manufacturing Technology (17-259-05-011 K), Open fund for Jiangsu Key Laboratory of Advanced Manufacturing Technology

(HGAMTL1601, HGAMTL-1703), National key research and development plan (2017YFB1103202) and Henan Key Research and Development Project (182102310629).

References

1. Álvarez JM et al (2014) Combining priors, appearance, and context for road detection. IEEE Transaction on intelligent transportation systems 15(3):1168–1178
2. Atangana A (2018) Application of stationary wavelet entropy in pathological brain detection. Multimedia Tools and Applications 77(3):3701–3714
3. Badrinarayanan V, Kendall A, Cipolla R (2017) SegNet: a deep convolutional encoder-decoder architecture for image segmentation. IEEE Transactions on Pattern Analysis & Machine Intelligence 39(12):2481–2495
4. Barsi A, Heipke C (2008) Artifical neural networks for the detection of road junctions in aerial images. Geol Mag 70(2):180–182
5. Byun J, Seo B-S, Lee J (2015) Toward accurate road detection in challenging environments using 3D point clouds. ETRI J 37(3):606–616
6. Chen M (2016) Morphological analysis of dendrites and spines by hybridization of ridge detection with twin support vector machine. PeerJ, 4, Article ID. e2207
7. Chen Y, Chen X-Q (2016) Sensorineural hearing loss detection via discrete wavelet transform and principal component analysis combined with generalized eigenvalue proximal support vector machine and Tikhonov regularization. Multimedia Tools and Applications 77(3):3775–3793
8. Chen Y, Lu H (2018) Wavelet energy entropy and linear regression classifier for detecting abnormal breasts. Multimedia Tools and Applications 77(3):3813–3832
9. Chen M, Li Y, Han L (2015) Detection of dendritic spines using wavelet-based conditional symmetric analysis and regularized morphological shared-weight neural networks. Computational and Mathematical Methods in Medicine: Article ID. 454076
10. Cheng J, Zhou X, Miller E, Witt RM, Zhu J, Sabatini BL, Wong STC (2007) A novel computational approach for automatic dendrite spines detection in two-photon laser scan microscopy. J Neurosci Methods 165(1):122–134
11. Dong D, Mcavoy TJ (1994) Nonlinear principal components analysis–based on principal curves and neural networks. Computers & Chemical Engineering 20(1):65–78
12. Du S (2016) Multi-objective path finding in stochastic networks using a biogeography-based optimization method. SIMULATION 92(7):637–647
13. Einbeck J, Dwyer J (2011) Using principal curves to analyse traffic patterns on freeways. Transportmetrica 7(3):229–246
14. Fan J, Zhou X, Dy JG, Zhang Y, Wong STC (2009) An automated pipeline for dendrite spine detection and tracking of 3D optical microscopy neuron images of in vivo mouse models. Neuroinformatics 7(2):113–130
15. Fan J et al. (2017) An automatic method for spine detection and spine tracking in in vivo images. in IEEE/ Nih Life Science Systems and Applications Workshop. Bethesda: IEEE. p. 233−+
16. Guo C, Mita S, McAllester D (2012) Robust road detection and tracking in challenging scenarios based on Markov random fields with unsupervised learning. IEEE Transaction on intelligent transportation systems 13(3):1338–1354
17. Jia W (2017) Three-Category Classification of Magnetic Resonance Hearing Loss Images Based on Deep Autoencoder. Journal of Medical Systems 41(10):Article ID. 165
18. Jiang YY (2017) Cerebral micro-bleed detection based on the convolution neural network with rank based average pooling. IEEE Access 5:16576–16583
19. Koh IY et al (2002) An image analysis algorithm for dendritic spines. Neural Comput 14(6):1283–1310
20. Kong H, Audibert J-Y, Ponce J (2010) General road detection from a single image. IEEE Transaction on intelligent transportation systems 19(8):2211–2220
21. Li Y, Cattani C (2017) Detection of dendritic spines using wavelet packet entropy and fuzzy support vector machine. CNS Neurol Disord Drug Targets 16(2):116–121
22. Li X, Zhang S, Pan X, Dale P, Cropp R (2010) Straight road edge detection from high-resolution remote sensing images based on the ridgelet transform with the revised parallel-beam radon transform. Int J Remote Sens 31(19):5041–5059
23. Li Y, Ding W, Zhang XG, Ju Z (2016) Road detection algorithm for autonomous navigation systems based on dark channel prior and vanishing point in complex road scenes. Robot Auton Syst 85(Supplement C):1–11
24. Liu AJ (2017) Tea category identification using computer vision and generalized eigenvalue proximal SVM. Fundamenta Informaticae 151(1–4):325–339
25. Long J, Shelhamer E, Darrell T (2015) Fully convolutional networks for semantic segmentation, in IEEE Conference on Computer Vision and Pattern Recognition. p. 3431–3440

26. Lu S, Lu Z (2018) A pathological brain detection system based on kernel based ELM. Multimedia Tools and Applications 77(3):3715–3728
27. Martínez Z, Ludeña C (2011) An algorithm for automatic curve detection. Computational Statistics & Data Analysis 55(6):2158–2171
28. Meijering E, Jacob M, Sarria JCF, Steiner P, Hirling H, Unser M (2004) Design and validation of a tool for neurite tracing and analysis in fluorescence microscopy images. Cytometry Part A 58A(2):167–176
29. Ozertem U, Erdogmus D (2011) Locally defined principal curves and surfaces. J Mach Learn Res 12(4):1249–1286
30. Pan H, Zhang C, Tian Y (2014) RGB-D image-based detection of stairs, pedestrian crosswalks and traffic signs. J Vis Commun Image Represent 25(2):263–272
31. Pulkkinen S (2015) Ridge-based method for finding curvilinear structures from noisy data. Computational Statistics & Data Analysis 82:89–109
32. Shi Q, Liu X, Li X (2017) Road detection from remote sensing images by generative adversarial networks. IEEE access, 2017. PP, DOI: 10.1109/ACCESS.2017.2773142
33. Shih FY, Kowalski AJ (2003) Automatic extraction of filaments in Hα solar images. Sol Phys 218(1–2):99–122
34. Silva G, Martins C, Moreira da Silva N, Vieira D, Costa D, Rego R, Fonseca J, Silva Cunha JP (2017) Automated volumetry of hippocampus is useful to confirm unilateral mesial temporal sclerosis in patients with radiologically positive findings. Neuroradiol J 30(4):318–323
35. Stanford DC, Raftery AE (2000) Finding curvilinear features in spatial point patterns: principal curve clustering with noise. IEEE Transactions on Pattern Analysis & Machine Intelligence 22(6):601–609
36. Su J, Srivastava A, Huffer FW (2013) Detection, classification and estimation of individual shapes in 2D and 3D point clouds: Elsevier Science Publishers B V. 227–241
37. Trevor Hastie WS (1989) Principal Curves. J Am Stat Assoc 84(406):502–516
38. Wei L, Yang J (2016) Fitness-scaling adaptive genetic algorithm with local search for solving the multiple depot vehicle routing problem. SIMULATION 92(7):601–616
39. Wu X (2018) Tea category identification based on optimal wavelet entropy and weighted k-nearest neighbors algorithm. Multimedia Tools and Applications 77(3):3745–3759
40. Xu XY et al. (2006) A shape analysis method to detect dendritic spine in 3D optical microscopy image. in 3rd IEEE International Symposium on Biomedical Imaging: Macro to Nano. Arlington: IEEE. p. 554–559
41. Zhan TM, Chen Y (2016) Multiple sclerosis detection based on biorthogonal wavelet transform, RBF kernel principal component analysis, and logistic regression. IEEE Access 4:7567–7576
42. Zhang Y, Zhou X, Witt RM, Sabatini BL, Adjeroh D, Wong STC (2007) Dendritic spine detection using curvilinear structure detector and LDA classifier. NeuroImage 36(2):346–360
43. Zhou H, Kong H, Wei L, Creighton D, Nahavandi S (2015) Efficient road detection and tracking for unmanned aerial vehicle. IEEE Trans Intell Transp Syst 16(1):297–309

Dr. Fanqiang Kong received the Ph.D. degree in information and communication engineering from Xidian University, Xi'an, China, in 2008. He is currently a lecturer at the College of Astronautics, Nanjing University of Aeronautics and Astronautics, Nanjing, China. His research interests include spectral image coding and image analysis, artificial intelligence, and pattern recognition

Dr. G. Vishnu Varthanan was born in Madurai district, Tamilnadu, India in the year 1986. He has completed his Bachelor of Engineering in Instrumentation and Control Engineering with first class in the year 2007 from Arulmigu Kalasalingam College of Engineering, Virudhunagar, Tamilnadu and Master of Technology with distinction in the year 2009 from Bharath University, Chennai, Tamilnadu. He has worked as a Lecturer in Electronics and Communication Engineering Department, Andal Alagar College of Engineering from May 2009 to June 2010. After gaining a year experience, he then joined as an Assistant Professor in Electrical and Electronics Engineering Department of Vels University, Pallavaram and he served there from June 2010 to May 2011. Later, he continued his academic service as an Assistant Professor in Electronics and Instrumentation Department of Kalasalingam University, since July 2011. He holds a PhD Degree awarded from the Department of Electronics and Communication Engineering and at present he is an Associate Professor in the Department of Instrumentation and Control Engineering of Kalasalingam University, Tamilnadu, India. His areas of interest are Medical image processing and signal processing, and he has significant publications pertaining to these domains

Prof. Yu-Dong Zhang received his Ph.D. degree from Southeast University at 2010. He worked as postdoc from 2010 to 2012, and a research scientist from 2012 to 2013 at Columbia University. He served as a full professor from 2013 to 2017 in Nanjing Normal University, where he was the director and founder of Advanced Medical Image Processing Group. He serves as Professor in University of Leicester, UK, from 2017 till now. He was included in “Most Cited Chinese researchers (Computer Science)” from 2015 to 2018. He was included in Top Scientist released by Guide2Research. He published over 100 papers, and 18 were included as “ESI Highly Cited Papers”. He has conducted many successful academic grants and industrial projects